Spatial Lipidomics Reveals Anticancer Mechanisms of Bufalin in Combination with Cinobufagin in Tumor-Bearing Mice

Jinghui Zhang[1], Yanjun Hong[2,3,4]*, Peisi Xie[2], Yang Chen[1], Lilong Jiang[2,3], Zhiyi Yang[2], Guodong Cao[2], Zhongjian Chen[1,5], Xuesong Liu[1], Yong Chen[1], Yongjiang Wu[1]* and Zongwei Cai[2]

[1]College of Pharmaceutical Sciences, Zhejiang University, Hangzhou, China, [2]Department of Chemistry, State Key Laboratory of Environmental and Biological Analysis, Hong Kong Baptist University, Hong Kong, China, [3]Shenzhen Research Institute and Continuing Education, Hong Kong Baptist University, Shenzhen, China, [4]School of Pharmaceutical Sciences (Shenzhen), Sun Yat-sen University, Shenzhen, China, [5]Cancer Research Institute, Zhejiang Cancer Hospital, Hangzhou, China

Bufalin (BFL) and cinobufagin (CBF) are the principal bioactive constituents of Chansu, a widely used traditional Chinese medicine (TCM). The synergistic effects of potential active components are responsible for the bioactivities of TCM. Our results showed that the cotreatment with BFL and CBF confers superior anticancer efficacy compared to monotreatment. To reveal the underlying mechanisms of their cotreatment, an integrated method composed of mass spectrometry-based lipidomics and matrix-assisted laser desorption/ionization mass spectrometry imaging was used to delineate the responses of tumor-bearing mice treated with BFL and CBF individually or in combination. The cotreatment with BFL and CBF modulated the sphingolipid metabolism and glycerophospholipid metabolism, and subsequently led to mitochondria-driven apoptosis and systemic disruption of biomembranes in tumor cells. Furthermore, we found that the disturbed lipid markers were mainly located in the non-necrotic tumor areas, the essential parts for the formation of solid tumor framework. Together, our findings revealed what occurred in tumor in response to the treatment of BFL and CBF, from lipids to enzymes, and thus provide insights into the critical role of lipid reprogramming in the satisfactory anticancer effect of BFL in combination with CBF.

Keywords: chansu, bufalin, cinobufagin, lipidomics, mass spectrometry imaging

INTRODUCTION

Hepatoma is a severe malignancy usually with poor prognosis (Thomas and Zhu, 2005). Although hepatoma can be surgically resected, chemotherapy has an irreplaceable status and function for patients in advanced stages (El-Serag et al., 2008). However, chemotherapy agents are still limited by many disadvantageous factors, such as side effects and drug resistance (Roth et al., 2013; Duncan, 2014). It is urgent to find more effective chemotherapeutic options. Chansu is obtained from the skin secretions of *Bufo bufo gargarizans* Cantor. Its extract has long been used as an anticancer agent in China and other Asian countries (Meng et al., 2009). Huachansu capsules, a sterilized extract of Chansu, has been marketed and used in clinical. They have been widely used for the treatment of

patients with various types of cancer, especially in liver cancer (Huang et al., 2020). The synergistic effects of the bioactive components account for the anticancer effects of Chansu and Huachansu. Bufadienolide-type cardiotonic steroids, bufalin (BFL) and cinobufagin (CBF) (**Supplementary Figure S1**), are the principal bioactive components in Chansu and Huachansu (Qi et al., 2011). We detected BFL and CBF in Huachansu capsules by ultra high performance liquid chromatography (**Supplementary Figure S2**). Their individual anticancer effects were associated with a downregulation of the pro-survival proteins Bcl-2, and an upregulation of the pro-apoptotic protein Fas and Bax (Qi et al., 2011; Shen et al., 2014). So far, the anticancer mechanisms of BFL and CBF were mostly assessed individually, which were insufficient for the guidance of their clinical joint use. Therefore, more emphasis should be put on the mechanisms of the combination of BFL and CBF.

Lipids play a fundamental role in maintaining membrane homeostasis, providing energy and are involved in cell signaling in all living cells (Ackerman et al., 2018; Storck et al., 2018). Accumulating evidence suggested that cancer was related to aberrant lipid metabolism (Hirsch et al., 2010; Deng and Li, 2020). Rapid proliferating cancer cells required increased lipid biosynthesis for the construction of membrane. And bioactive molecules produced by lipid catabolism acted as signal molecules in the regulation of cancer metastasis (Vander Heiden and DeBerardinis, 2017). As one important subfield of metabolomics, lipidomics investigate the holistic changes of endogenous lipids in response to stimuli based on analytical chemistry principles (Yang and Han, 2016). In view of the important role of lipid metabolism in cancer, lipidomics has been widely used in the diagnosis and treatment of cancer. For the diagnosis of cancer, the disorder of lipid metabolism occurred early in the tumor progression, which made lipids suitable to be used as diagnostic markers (Perrotti et al., 2016). For the treatment of cancer, understanding lipid metabolism pathways in cancer cells could provide potent targets for therapy, and elucidating the function of lipids could benefit the development of new anticancer drugs for clinical evaluation. Determining the lipid change induced by drugs could help to clarify the mechanism of drug action, and could provide a basis for the combination and efficacy improvement of drugs (Zhang et al., 2017; Brovkovych et al., 2018).

In addition to changes in the lipidomics, spatial information is essential to investigate subtle, highly localized changes of metabolites in histopathological regions of tumor. Therefore, advanced imaging techniques are needed for probing focal changes. Mass spectrometry imaging (MSI) is a powerful technique to simultaneously visualize the spatial distribution of molecules in biological samples. MSI has been widely utilized for the diagnostic and prognostic marker discovery (Sun et al., 2019), pharmacological target screening (Luo et al., 2013; He et al., 2015) and the investigation of the spatial distribution of metabolites, lipids and peptides in biological samples (Burnum et al., 2008; Muller et al., 2015; Li et al., 2020). In particular, lipids are appropriate for MSI analysis for several reasons: the polar head groups of many lipid species make their ionization

easier; they are abundant components of tissues; and most of them with a molecular weight within 300–1,000 Da (Zemski Berry et al., 2011).

In the present work, an enhanced anticancer effect was demonstrated by the cotreatment with BFL and CBF in the xenograft model. Their synergistic anticancer effect was obtained from cell culture experiments in our unpublished work. Our previous work demonstrated the metabolic regulation effects of the cotreatment of BFL and CBF *in vitro* (Zhang et al., 2020). To thoroughly investigate the underlying molecular mechanisms of their anticancer effects and reveal the possible target region, tumor-bearing mice were treated with BFL and CBF individually or in combination. Thereafter, lipid disturbance analysis was performed by liquid chromatography-mass spectrometry (LC-MS) based lipidomics combined with matrix-assisted laser desorption/ionization mass spectrometry imaging (MALDI-MSI). The findings of this work might provide a new insight to explore the anticancer mechanisms and localize the target region of BFL and CBF on the treatment of hepatoma.

METHOD

Chemicals and Materials

BFL and CBF with a purity over 98% were purchased from Chengdu Must Biotech Co., Ltd. (Chengdu, China). Cisplatin were purchased from Solarbio Biosciences Company (Beijing, China). Sinapic acid (SA), α-cyano-4-hydroxycinnamic acid (HCCA), 2,5-dihydroxybenzoic acid (DHB), peptides and N-(1-naphthyl)-ethylenediamine dihydrochloride (NEDC) were purchased from Sigma-Aldrich (MO). Phosphate-buffered saline (PBS) was purchased from GIBCO (Grand Island, NY). Human hepatoma cell line HepG2 was purchased from Cobioer Biosciences Company (Nanjing, China).

Establishment of Tumor Nude Mice Model (Tumor Xenografts) and Drug Administration

Male 4–6 weeks-old BALB/c nude mice were purchased from the Chinese University of Hong Kong. All mice were maintained in sterile individually ventilated cages. Water and food were available ad libitum. The lights were on for 12 h per day, and the temperature was kept at $20 \pm 2°C$ with humidity of $45 \pm 10\%$. After 7 days of adaptation period, 5×10^6 of HepG2 cells were subcutaneously implanted into the armpit of each mouse. When the tumor size reached $100 \, mm^3$, the mice were randomly divided into five groups (eight mice per group), mice in different groups received drugs or PBS by intraperitoneal injection: 1) BFL 2 mg/kg, once a day, 2) CBF 4 mg/kg, once a day, 3) BFL 2 mg/kg + CBF 4 mg/kg, once a day, 4) Cisplatin 3 mg/kg, twice a week (positive control), and 5) PBS (negative control). The body weight and tumor volume were measured every two days. The tumor volume was calculated by the formula: $V = 0.5 \times a \times b^2$, where a and b represent the length and width of the tumor, respectively. After 3 weeks, the mice were sacrificed. Tumors were

collected and weighed, then stored at -80°C for LC-MS and MALDI-MSI analysis. The detailed schedule for the xenograft tumor model is shown in **Figure 1A**.

Enzyme-Linked Immunosorbent Assay to Measure AFP in Serum

Mouse blood samples were collected and incubated for 30 min at room temperature before centrifuging for 20 min at 2000 g. The supernatant serum was carefully collected after centrifugation. AFP ELISA kit was purchased from Meimian Industrial Co., Ltd. (Jiangsu, China). The serum levels of AFP were measured according to the vendor's instructions.

Interaction of Bufalin and Cinobufagin

Bliss independence is widely used to analyze drug interaction. The method compares the observed combination effect (Y_O) with the predicted combination effect (Y_P) (Bliss, 1939). Typically, the combination effect is declared synergistic if Y_O is greater than Y_P.

For statistical calculation, the relation between drug effect and concentration of AFP was described as the following equation:

$$Y = 1 - \frac{\text{AFP}_{\text{treated}}}{\text{AFP}_{\text{control}}}$$

where Y is the effect of drugs; $\text{AFP}_{\text{treated}}$ and $\text{AFP}_{\text{control}}$ are the concentration of AFP in the serum of treated group and PBS group, respectively.

According to Bliss independence, the combination effect for BFL and CBF can be predicted as:

$$Y_P = Y_{\text{BFL}} + Y_{\text{CBF}} - Y_{\text{BFL}}Y_{\text{CBF}}$$

Where Y_{BFL} and Y_{CBF} are the effect of BFL and CBF, respectively.

Lipidomics Analysis

Ten mg of tumor tissue was mixed with 320 µL of ice-cold MeOH/H$_2$O (80:20, v/v) and homogenized using a Polytron PT2100 homogenizer (Kinematica, Lucerne, Switzerland). Subsequently, 1 ml of MTBE was added and vortexed for 1 min. A total of 200 µL of water was added to induce phase separation. Sample was vortexed for 1 min and incubated at room temperature for 5 min. After centrifugation at 12,000 g and −4°C for 15 min, the upper phase was collected and dried at 4°C.

The lipidomic analysis was performed using an Ultimate 3,000 ultra-high performance liquid chromatograph (UHPLC, Dionex, Sunnyvale, CA) coupled with an Orbitrap Fusion Tribrid mass spectrometer (Thermo Fisher Scientific Inc., Waltham, MA). Lipid separation was performed on an ACQUITY UPLC BEH C18 column (2.1 mm × 100 mm, 1.7 µm, Waters, Milford, MA). The details of mobile phase for UHPLC and MS parameters are summarized in **Supplementary Table S1**.

The raw data were processed by LipidSearch software (Thermo Fisher Scientific Inc., Waltham, MA) for extraction, alignment and identification of the lipids. The multivariate statistical analysis was processed using SIMCA software (Version 14.1, Umetrics, Sweden). Orthogonal partial least squares discriminant analysis (OPLS-DA) and Student's *t*-test were performed. The *p*-value and fold change (FC) were calculated from the peak area. The differential lipids between the control and drug treated groups were selected based on the variable importance in projection (VIP) value (VIP >1), *p* value (*p* < 0.05) as well as fold change (FC > 1.2 or <0.8).

Quantitative Real-Time Polymerase Chain Reaction

Total RNA was extracted from tumor tissue using the RNAiso plus kit (TaKaRa, Japan). cDNAs were synthesized using the PrimeScript RT reagent kit (Takara, Japan). Quantitative PCR was performed using SYBR Premix Ex Taq (Takara, Japan) on Piko Real-Time PCR system (Thermo Scientific, Waltham, MA). Statistical analysis was conducted by GraphPad Prism five Software, Inc. (La Jolla, CA).

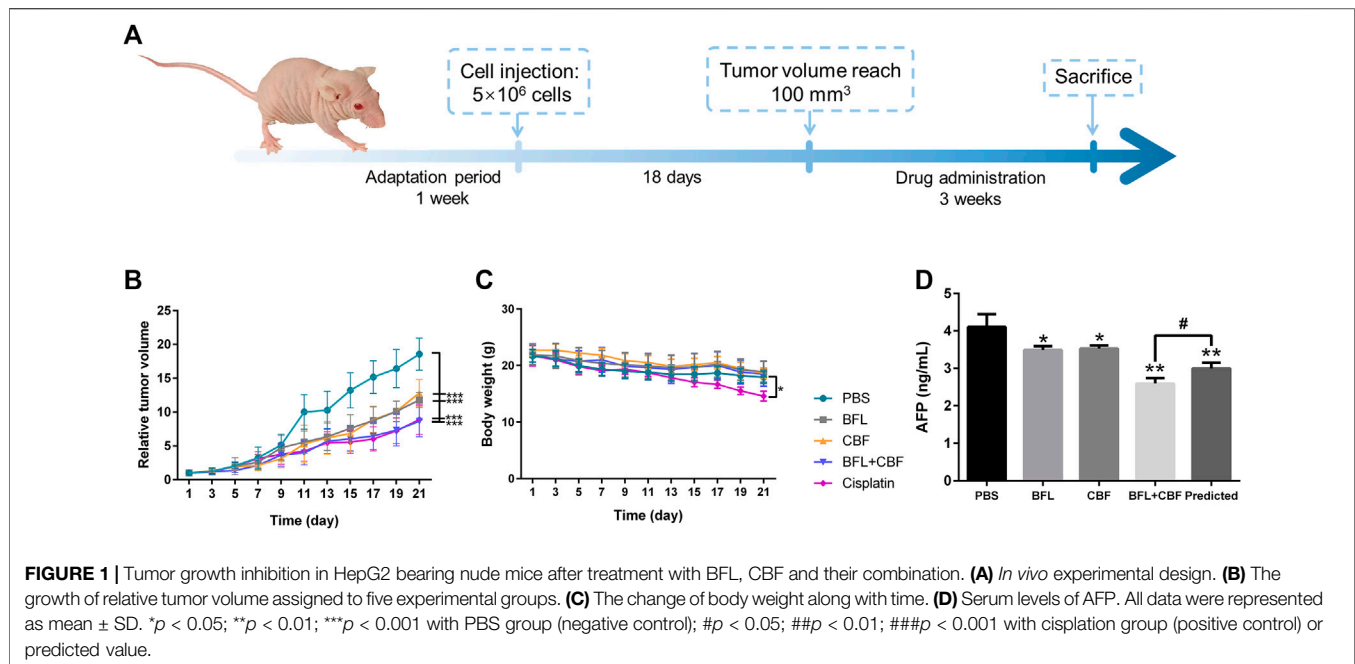## Lipid Imaging by Matrix-Assisted Laser Desorption/Ionization Mass Spectrometry Imaging

The 14-µm-thick tumor tissue sections were cut using a CryoStar Nx70 cryostat (Thermo Fisher Scientific, Walldorf, Germany) at -20 °C. The slices were dried in a vacuum desiccator for 20 min before MALDI-MSI analysis. Matrix was prepared using an automatic matrix sprayer (ImagePrep, Bruker Daltonics, Billerica, MA), as described by Wang et al. (Wang et al., 2015). Serial tumor tissue sections were subsequently stained using hematoxylin and eosin (H&E) for pathological examination. MALDI-MSI was carried out using a rapifleX MALDI Tissuetyper (Bruker Daltonics, Germany) equipped with a smartbeam laser in the M5 mode. The mass spectra were acquired at a mass range of m/z 250–1,200 in the negative ionization mode by averaging signal from 1,000 shots at 3.0 × 2810 V of detector gain and 82% of laser power. The other parameters were optimized, including lens voltage (11.00 kV), reflector voltage (20.84 kV), pulsed ion extraction time (100 ns) and ion source voltage (20 kV). The spatial resolution for MALDI-MSI was set at 100 µm. The instrument calibration was performed with external standards (SA, DHB, HCCA, and Peptides) before each data acquisition.

The obtained MALDI-MSI raw data were firstly processed and analyzed by FlexImaging 5.0 software (Bruker Daltonics, Germany), and subsequently imported into SCiLS Lab 2016a software (Bruker Daltonics, Germany) for multivariate statistical analysis.

RESULTS

Anticancer Effect of Bufalin, Cinobufagin and Their Cotreatment

The antitumor efficacy of BFL, CBF and their combination was investigated in HepG2 tumor-bearing mice using cisplatin as a positive control and PBS as a negative control. As shown in **Figure 1B**, the tumor volume in the negative control group increased rapidly. When used separately, BFL and CBF displayed a significant tumor growth inhibition. The

FIGURE 1 | Tumor growth inhibition in HepG2 bearing nude mice after treatment with BFL, CBF and their combination. **(A)** *In vivo* experimental design. **(B)** The growth of relative tumor volume assigned to five experimental groups. **(C)** The change of body weight along with time. **(D)** Serum levels of AFP. All data were represented as mean ± SD. *$p < 0.05$; **$p < 0.01$; ***$p < 0.001$ with PBS group (negative control); #$p < 0.05$; ##$p < 0.01$; ###$p < 0.001$ with cisplation group (positive control) or predicted value.

cotreatment with BFL and CBF led to stronger inhibition of tumor growth, which is similar to the therapeutic efficacy of cisplatin. Weight loss is a serious side effect of chemotherapy that decreases the prognosis of cancer patients (Garcia et al., 2013). **Figure 1C** showed that neither monotreatment nor cotreatment with BFL and CBF induced significant body weight change for mice. However, we observed the loss of body weight in the cisplatin treated group, which is consistent with previous reports (Garcia et al., 2013; Su et al., 2014). α-fetoprotein (AFP) was one of the most important indicators for hepatoma (Woodfield et al., 2017). Elevated serum levels of AFP have been reported to positively correlate with cancer deterioration (Ortega et al., 2000) Previous study has demonstrated that silencing AFP expression induces apoptosis in hepatoma cell (Yang et al., 2008). As shown in **Figure 1D**, the predicted concentration of AFP is significantly higher than the observed concentration, that indicating the combination of BFL and CBF induced superior effect than predicted. Their synergetic effect was verified.
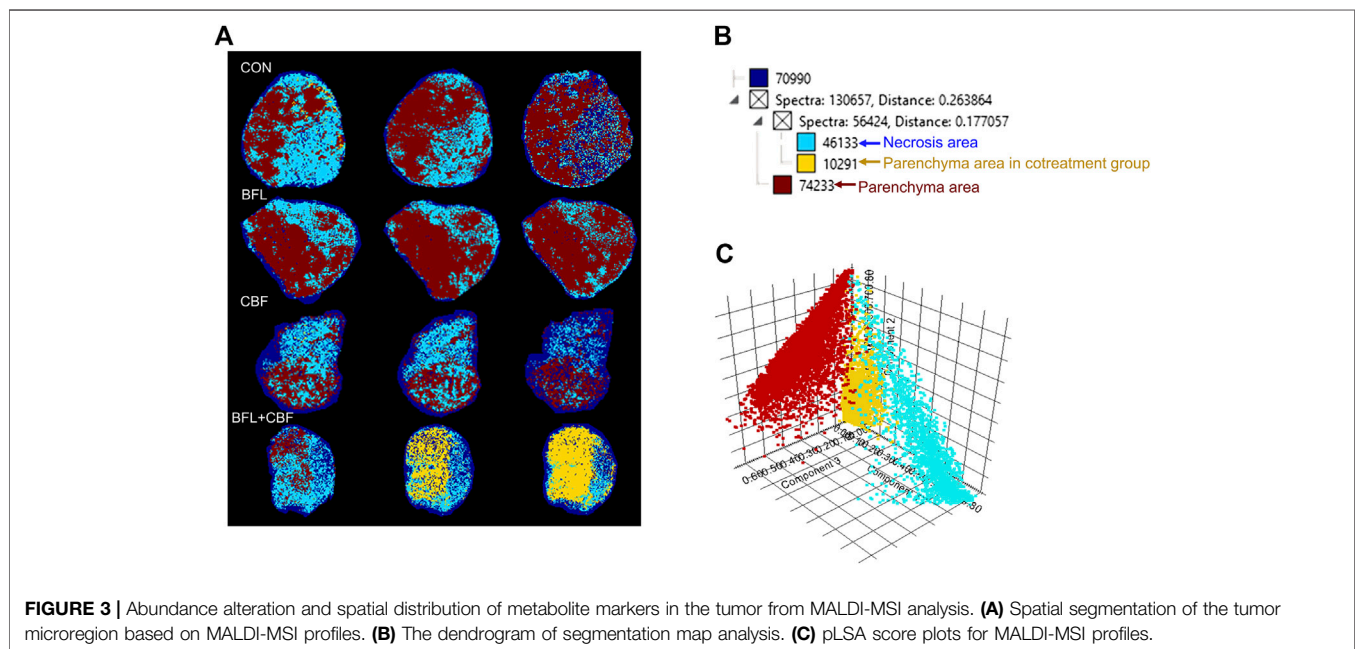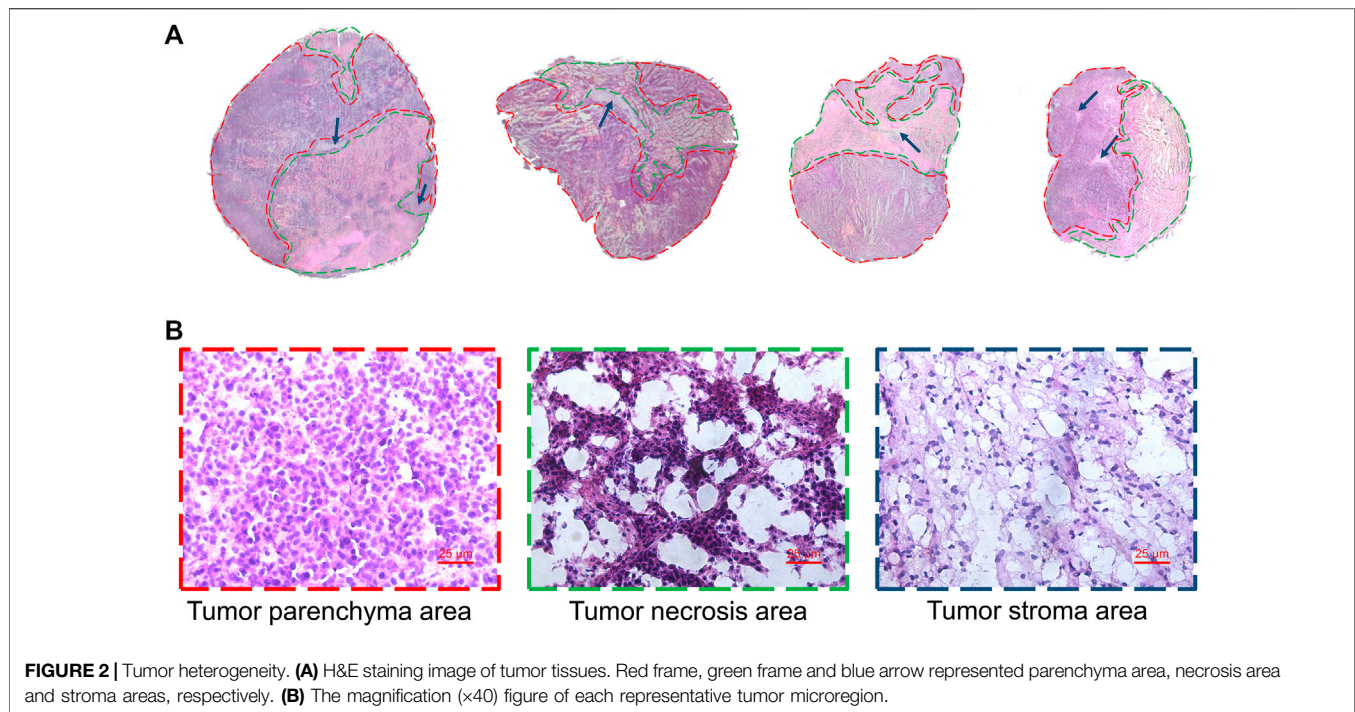
Global Metabolic Shifts Induced by Drug Treatment

Heterogeneity is one of the characteristics of malignant tumors, including intratumor morphological diversity and heterogeneity for drug sensitivity (Bae and Park, 2011; Zhang et al., 2014). As shown in **Figure 2**, the histopathological results indicated considerable spatial heterogeneity in tumor morphology. The parenchyma areas (red frame) and stroma areas (blue arrow) (Bae, 2009), are important in the formation of a firm tumor framework. According to the cell morphology, the tumor necrosis area (green frame) can be determined by the notable cellular debris. To understand the changes in tumor metabolic profile and visualize the histological regions, the spectra from ion signal

profiles were processed by SCiLS Lab software and separated using spatial segmentation analysis and probabilistic latent semantic analysis (pLSA). All spectra of the particular cluster were displayed as a spatial segmentation map, and all pixels in the map were colored according to their cluster assignments. As shown in **Figure 3A**, the bright blue cluster and red cluster corresponded to the tumor necrosis areas and parenchyma areas, respectively. The results of MSI segmentation were consistent with the H&E staining results (**Figures 2A,3A**). Interestingly, the yellow cluster could only be found in the tumor parenchyma areas of the cotreatment group. According to dendrogram and pLSA (**Figures 3B,C**), bright blue region and yellow region were separated from the same cluster, indicating their close correlation. The phenomenon might relate to the metabolic dysfunction induced by the cotreatment of BFL and CBF.

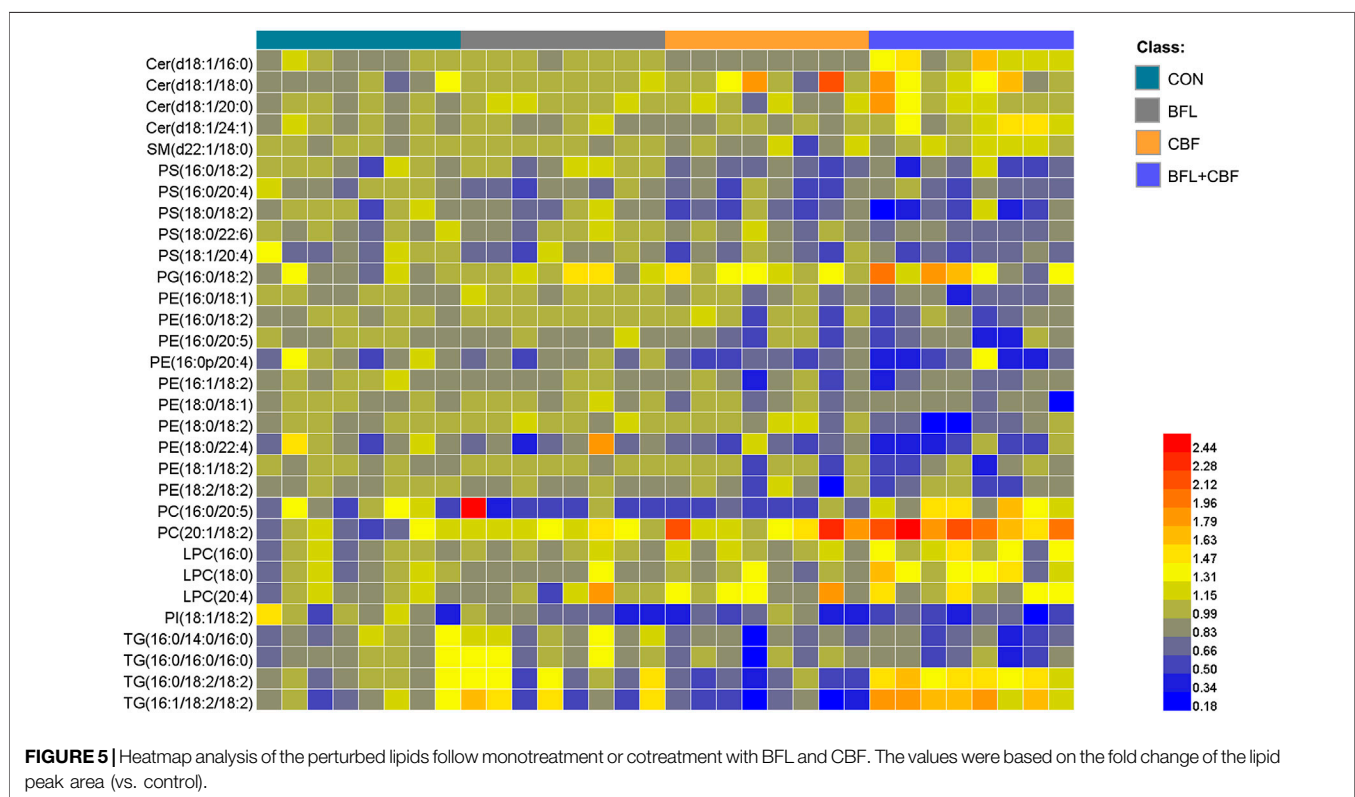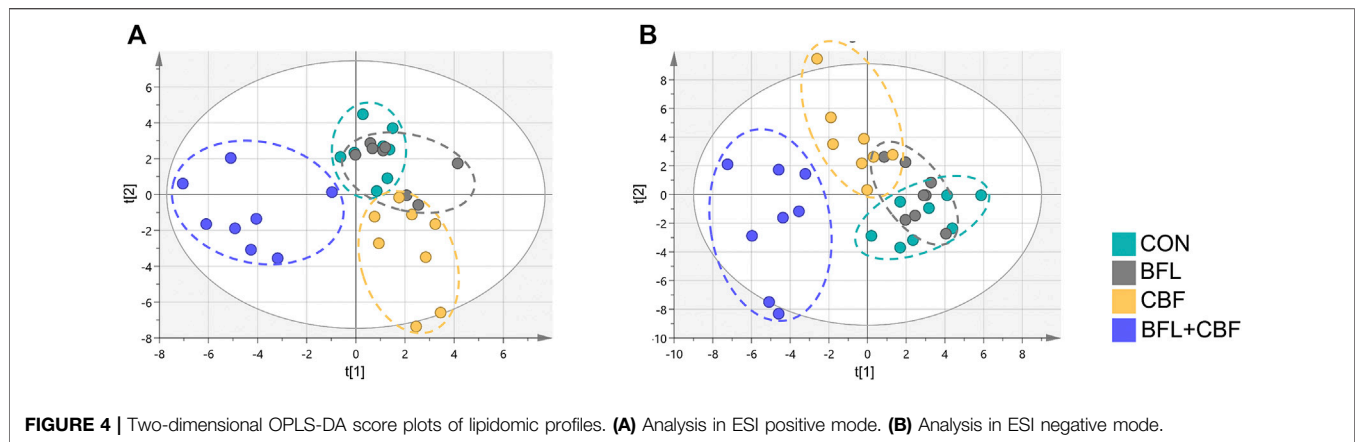## Global Metabolic Shifts Induced by Drug Treatment

The lipidomic profiles of tumor tissue were acquired using UHPLC-MS/MS under positive and negative ionization modes. 915 ions in ESI (+) and 426 ions in ESI (−) were obtained. OPLS-DA score plots were performed for discriminating between groups. **Figure 4** showed the segregation of drug treated groups and the control group. When BFL and CBF were used in combination, distinct differences were observed between cotreatment group and control group, suggesting that the combination of BFL and CBF induced conspicuous perturbation of lipids. A total of 31 perturbed lipids primarily contributed to the separation of BFL + CBF group and control group (**Figure 5** and **Supplementary Table S2**). The main perturbed lipids were sphingolipids (SPs) and glycerophospholipids (GPs).

FIGURE 2 | Tumor heterogeneity. (A) H&E staining image of tumor tissues. Red frame, green frame and blue arrow represented parenchyma area, necrosis area and stroma areas, respectively. (B) The magnification (×40) figure of each representative tumor microregion.

FIGURE 3 | Abundance alteration and spatial distribution of metabolite markers in the tumor from MALDI-MSI analysis. (A) Spatial segmentation of the tumor microregion based on MALDI-MSI profiles. (B) The dendrogram of segmentation map analysis. (C) pLSA score plots for MALDI-MSI profiles.

Sphingolipid Metabolism

Ceramide (Cer) that played important roles in SP metabolism was significantly increased by BFL + CBF cotreatment (**Figure 6A**). Cer could be formed either by ceramide synthase (CERS) catalyzed *de novo* synthesis, or through the sphingomyelinase (SMase) dependent hydrolysis of sphingomyelin (SM) (Reynolds et al., 2004). The reaction could proceed in the reverse orientation. The enzyme responsible for SM synthesis was sphingomyelin synthase (SMsynthase), which catalyzed the transfer of a phosphocholine from phosphatidylcholines (PC) to the primary hydroxyl group of Cer forming SM (Ullman and Radin, 1974). The catabolism of Cer proceeded through the action of a ceramidase (CDase), which hydrolyzed the amide bond, thus releasing the sphingoid base and free fatty acid (Mao and Obeid, 2008). As shown in **Figure 6B**, the cotreatment with BFL and CBF elevated the transcript level of CERS, but

FIGURE 4 | Two-dimensional OPLS-DA score plots of lipidomic profiles. **(A)** Analysis in ESI positive mode. **(B)** Analysis in ESI negative mode.

FIGURE 5 | Heatmap analysis of the perturbed lipids follow monotreatment or cotreatment with BFL and CBF. The values were based on the fold change of the lipid peak area (vs. control).
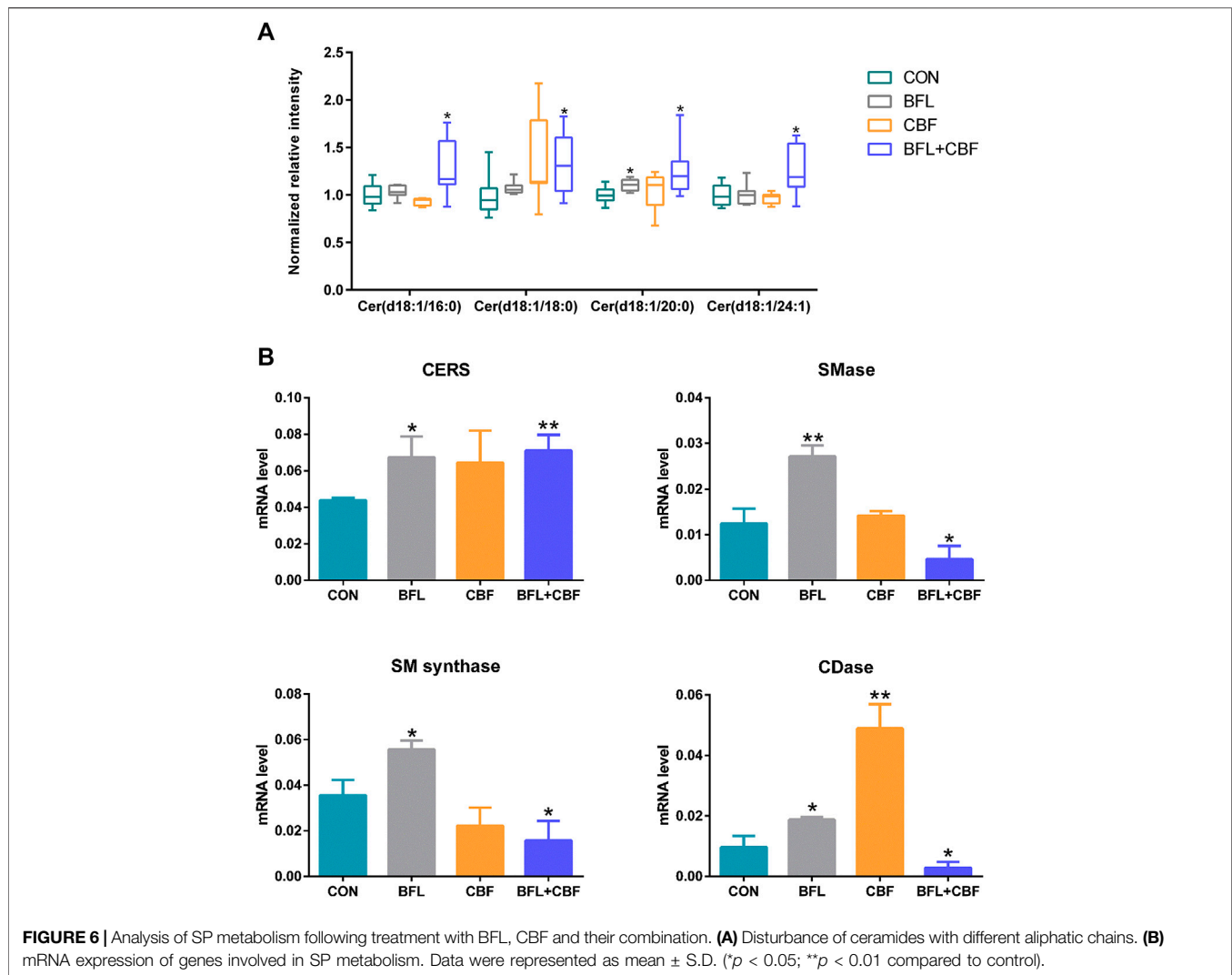
suppressed the conversion between Cer and SM. These promoted the biosynthesis of Cer. In parallel to facilitated Cer synthesis, the combination of BFL and CBF suppressed CDase (involved in Cer catabolism). However, the different trend was observed with SMase, SMsynthase and CDase, when BFL and CBF were used individually.

Glycerophospholipid Metabolism

Among GPs, the abundance of identified lipids exhibited remarkable upregulation in phosphatidylglycerol (PG), PC and lysophosphatidylcholine (LPC) as well as significant downregulation in phosphatidylserine (PS), phosphatidylethanolamine (PE) and

phosphatidylinositol (PI) in the cotreatment group (**Figure 7A**). To delineate the alteration of key enzymes in the pharmacological actions, the expression of involved genes was determined by qPCR. In GP metabolism, PE was synthesized either by the diacylglycerol ethanolaminephosphotransferase (EPT) catalyzed cytidine diphosphate (CDP)-ethanolamine (Kennedy) pathway or by the phosphatidylserine decarboxylase (PSD) catalyzed PS decarboxylation (Hermansson et al., 2011). All mammalian cells synthesized PC via the 1,2-diacylglycerol cholinephosphphotransferase (CPT) catalyzed CDP-choline (Kennedy) pathway, but hepatocytes could also produce PC by phosphatidylethanolamine N-methyltransferase (PEMT) catalyzed

FIGURE 6 | Analysis of SP metabolism following treatment with BFL, CBF and their combination. **(A)** Disturbance of ceramides with different aliphatic chains. **(B)** mRNA expression of genes involved in SP metabolism. Data were represented as mean ± S.D. (*$p < 0.05$; **$p < 0.01$ compared to control).

methylation of PE (Vance et al., 1997). PS was synthesized by phosphatidylserine synthase (PSS) one and two from PC and PE, respectively (Vance and Steenbergen, 2005). Phosphatidylglycerol synthase (PGS) catalyzed the reaction involved in the synthesis of PG (Huang and Freter, 2015). As shown in **Figure 7B**, the cotreatment of BFL and CBF upregulated the expression of PSD and PEMT, and downregulated the expression of PSS1. However, the expression of EPT, CPT, PSS2 and PGS were not significantly changed (**Supplementary Figure S3**).
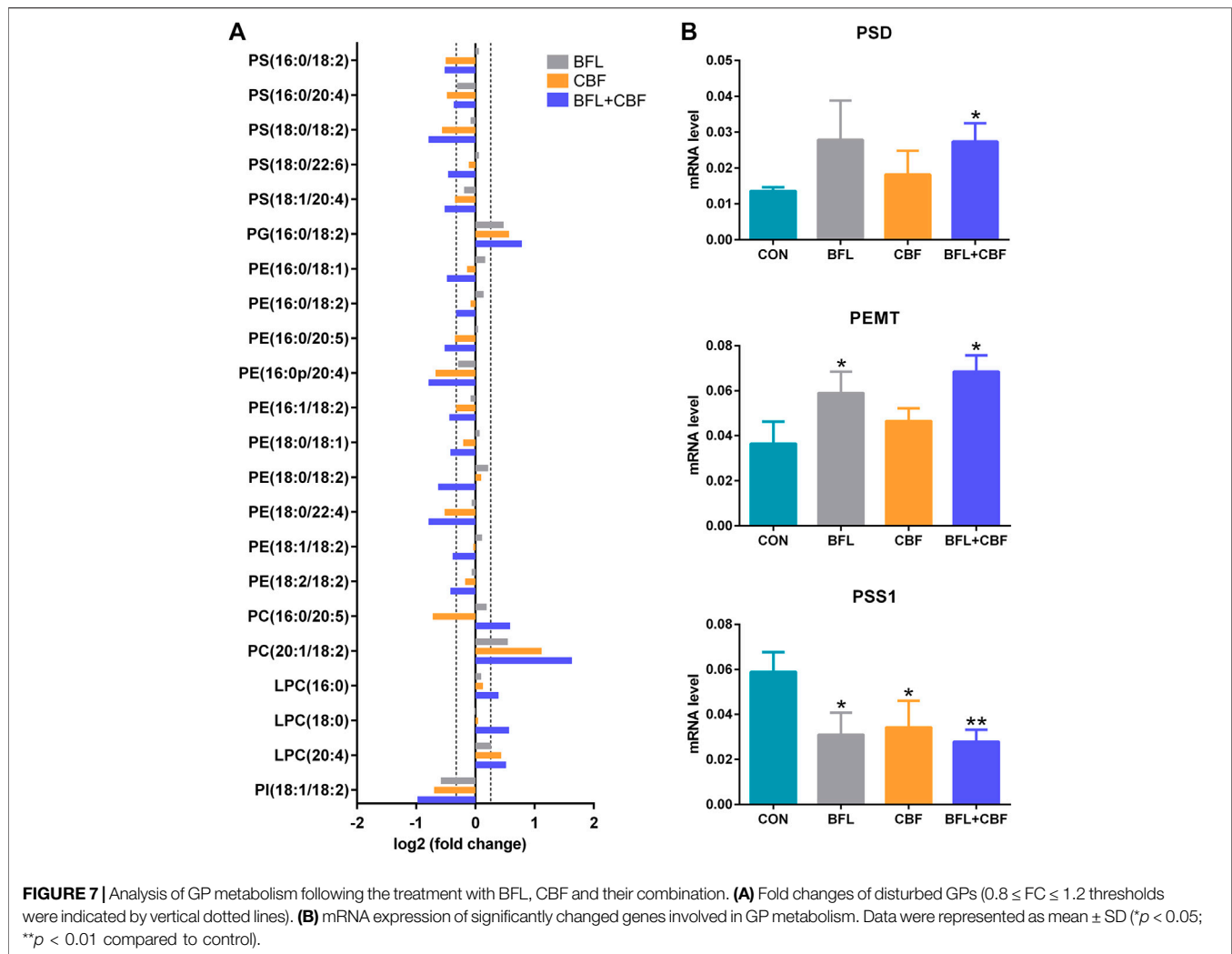
Visualization and Localization of Anticancer Lipid Biomarkers

MALDI-MSI was used to visualize the spatial distribution of anticancer lipid markers in tumor sections (**Figure 8**). With the treatment of BFL and CBF individually or in combination, four lipids were found to be significantly altered, which mainly distributed in the parenchyma areas and stroma areas of the tumor. Compared with control group, ion intensities of

PC (20:1/18:2) and PG (16:0/18:2) were significantly increased, whereas decreased abundances of PE (18:2/18:2) and PS (16:0/20:4) were found.

DISCUSSION

Hepatoma is a severe malignancy in the world with high morbidity and mortality. Despite all the medical efforts, it remains radically incurable, especially for advanced cases (Schütte et al., 2014). The low efficiency of single agent is an important reason for this unfavorable situation. Combination therapy has been successfully applied in reducing side effects and achieving enhanced effectiveness (Lehár et al., 2009). The data presented herein showed that the cotreatment with BFL and CBF enhanced the antitumor efficacy in the xenograft mouse model but did not induced significant loss in body weight. As a typical side effect of chemotherapy, weight loss could negatively influence treatment outcomes, even in overweight people (Arends et al., 2017).

FIGURE 7 | Analysis of GP metabolism following the treatment with BFL, CBF and their combination. **(A)** Fold changes of disturbed GPs ($0.8 \leq FC \leq 1.2$ thresholds were indicated by vertical dotted lines). **(B)** mRNA expression of significantly changed genes involved in GP metabolism. Data were represented as mean ± SD (*$p < 0.05$; **$p < 0.01$ compared to control).

With satisfactory efficiency and low side effect, the combination of BFL and CBF was suitable for cancer therapy. To thoroughly clarify their pharmacological mechanisms, a spatial lipidomics approach that aligns well with the complexity and integrity of combination therapy was used to provide insights into the responses of tumor toward the drug combination treatment. The spatial lipid shifts induced by drug treatment were visualized by MALDI-MSI. Interestingly, tumor parenchyma area in the cotreatment group showed similar metabolic profile with necrosis areas of other groups. But the metabolic profile between parenchyma area and necrosis areas are totally different in the monotreatment group (**Figures 2**, **3**). This indicated the transformation of tumor parenchyma areas to necrosis areas, which could benefit the therapy and prognosis of cancer.

LC-MS based lipidomics was performed to find the lipid markers. The disorder of SPs and GPs was found to have a close relationship with the satisfactory anticancer effect of BFL in combination with CBF:

Of particular interest in lipidomic results was the accumulation of ceramides in SP metabolism (**Figure 6A**)

due to the intimate connection between ceramides and apoptosis (D Mullen and M Obeid, 2012; Li et al., 2014). The stimulated expression of Cer synthesis related gene and the suppressed expression of catabolism related gene jointly led to the accumulation of Cer in the contreatment group. Moreover, sufficient amounts of SM supported Cer biogenesis, although their interconversion catalyzed by SMases and SMsynthase was not upregulated. Increased Cer level was observed in response to many cancer chemotherapeutic agents, including fludarabine, vincristine, etoposide, daunorubicin, irinotecan, paclitaxel, fenretinide and doxorubicin (Senchenkov et al., 2001). Ceramide triggered the mitochondria-driven apoptosis (Won and Singh, 2006). Specifically, ceramide induced the release of cytochrome *c*, an electron carrier of the mitochondrial electron-transport chain (Andrieuabadie et al., 2001; Ow et al., 2008). The release of cytochrome *c* led to a decrease in mitochondrial inner transmembrane potential (ΔΨm), mitochondrial oxygen consumption and Ca^{2+} retention, and all of which caused mitochondrial dysfunction and ROS generation, ultimately induced apoptosis (Ghafourifar et al., 1999) (**Figure 9**). Our
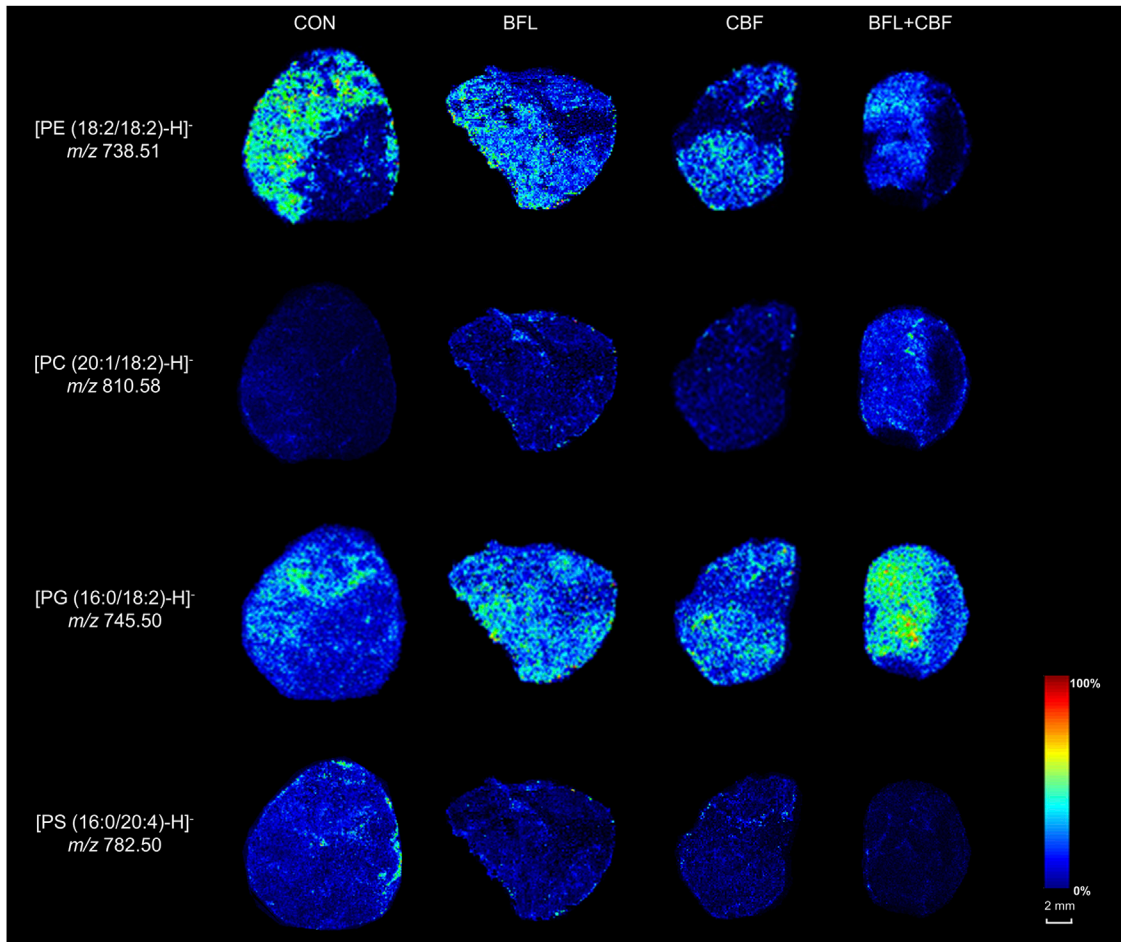
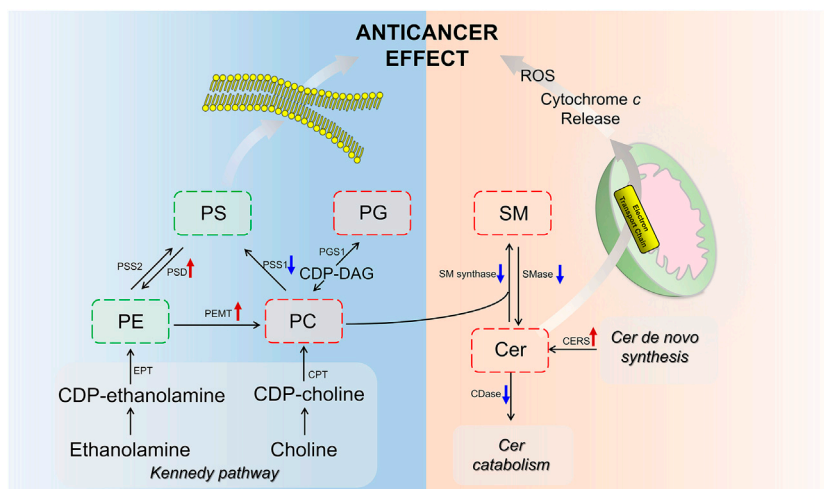**FIGURE 8 |** MALDI-MSI images of lipid markers in tumor sections.

FIGURE 9 | Scheme of perturbed lipid pathways. Lipids and genes marked in red (up arrow) and green (down arrow) represented the up- and downregulation, respectively.

findings indicated that the pro-apoptosis effect of BFL in combination with CBF was mediated in part through the accumulation of ceramide. The inconsistent regulation between monotreatment and cotreatment groups on the conversion between Cer and SM as well as the catabolism of Cer might be a potential mechanism for their synergistic effect.

GPs are the major structural lipids, which elicit crucial biological functions in membrane integrity and functional lipid biosynthesis (Hishikawa et al., 2014). After the cotreatment with BFL and CBF, the abundance of PC was increased, whereas the levels of PE and PS were decreased. This finding indicated that the cotreatment with BFL and CBF promoted the methylation from PE to PC, but not the conversion from PC to PS, which was verified by the activation of PEMT and suppression of PSS1. Besides, PC was also the substrate for SMase to form SM in SP metabolism, and the inhibition of SMase contributed to the accumulation of PC (**Figure 9**). Consequently, the level of PC was increased. PC induces apoptosis of hepatoma cells via death ligands (Sakakima et al., 2009). Additionally, PE and PC were the major constituents of biological membranes, and contributed to cell proliferation (Gibellini and Smith, 2010). The metabolic disorders of PE and PC might lead to the disruption of cell membrane homeostasis (Vance, 2013). PG was a biosynthetic precursor of cardiolipin, located in the inner mitochondrial membrane and was required for the function of many of the respiratory and ATP synthesizing enzymes (Struzik et al., 2020). The increase of PG suggested that the treatment of BFL and CBF might disturb the structure of mitochondrial membrane. Our results showed that the treatment of BFL and CBF induced a dysregulation of GP metabolism in the tumor, which might result in the instability of biomembranes and produce anticancer efficacy (**Figure 9**).

To verify the variation of lipid abundance and investigate the therapeutic target of BFL and CBF, we used MALDI-MSI to visualize the spatial distribution of lipid markers in tumor tissue. We found the disturbed lipid markers mainly located in the tumor parenchyma areas and stroma areas. It demonstrated the tumor parenchyma areas and stroma areas (essential parts for the formation of solid tumor framework) were sensitive targets for BFL and CBF (**Figures 2**, **8**). The spatial distribution of drugs in tumor is related to tumor heterogeneity and influencing clinical outcomes (De Maar et al., 2020). The distribution of many drugs was detected by MSI (Lukowski et al., 2017; Strydom et al., 2019). Giordano et al. (Giordano et al., 2016) measured the distribution of paclitaxel, a wildly used anticancer drug, in xenograft mouse model. Mice were treated with paclitaxel intravenously at a single dose of 60 mg/kg. They found paclitaxel accumulated in the non-necrotic tumor areas. However, in our research, mice were treated with 2 mg/kg of BFL and 4 mg/kg of CBF via intraperitoneal injection for 21 days. The doses were too low to be detected in the tumor tissue. In our future work, experiments with higher doses will be performed for the research of the distribution of BFL and CBF in the tumor.

CONCLUSION

Together, the present study demonstrated that the combination of BFL and CBF acted synergistically in inducing apoptosis and inhibiting growth in xenograft tumor. A novel mass spectrometry-based spatial lipidomic method was applied to reveal the underlying mechanism. As indicated by MALDI-MSI study, the drugs may penetrate into tumor and act in non-necrotic tumor areas. Our results indicated that the metabolism dysregulation of SPs and GPs with the treatment of BFL and CBF led to mitochondria-driven apoptosis and systemic disruption of biomembranes. In particular, the discrepant regulation of related enzymes in sphingolipid metabolism among the monotreatment and cotreatment with BFL and CBF might account for their synergism. This study provides theoretical basis for the combination of BFL and CBF in clinical practice.

DATA AVAILABILITY STATEMENT

The raw data supporting the conclusion of this article will be made available by the authors, without undue reservation, to any qualified researcher.

ETHICS STATEMENT

The animal study was reviewed and approved by Hong Kong Special Administrative Region Department of Health (License number: (19-32) in DS/SHS/8/2/6 Pt.3).

AUTHOR CONTRIBUTIONS

YW and ZWC conceived the idea. YH designed the study. JZ performed the experimental work and drafted the manuscript. PX conducted the MSI analysis. LJ participated in the animal experiment. YaC and ZJC participated in data analysis. ZY and GC participated in the lipidomic analysis. XL and YoC revised the manuscript. All authors read and approved the final manuscript.

FUNDING

SUPPLEMENTARY MATERIAL

The Supplementary Material for this article can be found online at: https://www.frontiersin.org/articles/10.3389/fphar.2020.593815/full#supplementary-material.

REFERENCES

Ackerman, D., Tumanov, S., Qiu, B., Michalopoulou, E., Spata, M., Azzam, A., et al. (2018). Triglycerides promote lipid homeostasis during hypoxic stress by balancing fatty acid saturation. *Cell Rep.* 24 (10), 2596–25e5. doi:10.1016/j.celrep.2018.08.015

Andrieuabadie, N., Gouazé, V., Salvayre, R., and Levade, T. (2001). Ceramide in apoptosis signaling: relationship with oxidative stress. *Free Radic. Biol. Med.* 31 (6), 717–728. doi:10.1016/s0891-5849(01)00655-4

Arends, J., Baracos, V., Bertz, H., Bozzetti, F., Calder, P., Deutz, N. E. P., et al. (2017). ESPEN expert group recommendations for action against cancer-related malnutrition. *Clin. Nutr.* 36 (5), 1187–1196. doi:10.1016/j.clnu.2017.06.017

Bae, Y. H., and Park, K. (2011). Targeted drug delivery to tumors: myths, reality and possibility. *J. Contr. Release.* 153 (3), 198. doi:10.1016/j.jconrel.2011.06.001

Bae, Y. H. (2009). Drug targeting and tumor heterogeneity. *J. Contr. Release.* 133 (1), 2. doi:10.1016/j.jconrel.2008.09.074

Bliss, C. I. (1939). The toxicity of poisons applied jointly. *Ann. Appl. Biol.* 26 (3), 585–615. doi:10.1111/j.1744-7348.1939.tb06990.x

Brovkovych, V., Izhar, Y., Danes, J. M., Dubrovskyi, O., Sakallioglu, I. T., Morrow, L. M., et al. (2018). Fatostatin induces pro-and anti-apoptotic lipid accumulation in breast cancer. *Oncogenesis.* 7 (8), 1–10. doi:10.1038/s41389-018-0076-0

Burnum, K. E., Frappier, S. L., and Caprioli, R. M. (2008). Matrix-assisted laser desorption/ionization imaging mass spectrometry for the investigation of proteins and peptides. *Annu. Rev. Anal. Chem.* 1, 689–705.doi:10.1146/annurev.anchem.1.031207.112841

D Mullen, T., and M Obeid, L. (2012). Ceramide and apoptosis: exploring the enigmatic connections between sphingolipid metabolism and programmed cell death. *Anticancer Agents Med Chem.* 12 (4), 340–363. doi:10.2174/187152012800228661

De Maar, J. S., Sofias, A. M., Siegel, T., Vreeken, R. J., Moonen, C., Bos, C., et al. (2020). Spatial heterogeneity of nanomedicine investigated by multiscale imaging of the drug, the nanoparticle and the tumour environment. *Theranostics.* 10 (4), 1884. doi:10.7150/thno.38625

Deng, H., and Li, W. (2020). Monoacylglycerol lipase inhibitors: modulators for lipid metabolism in cancer malignancy, neurological and metabolic disorders. *Acta Pharm. Sin. B.* 10 (4), 582–602. doi:10.1016/j.apsb.2019.10.006

Duncan, R. (2014). Polymer therapeutics: top 10 selling pharmaceuticals—what next?. *J. Contr. Release.* 190, 371–380. doi:10.1016/j.jconrel.2014.05.001

El-Serag, H. B., Marrero, J. A., Rudolph, L., and Reddy, K. R. (2008). Diagnosis and treatment of hepatocellular carcinoma. *Gastroenterology.* 134 (6), 1752–1763. doi:10.1053/j.gastro.2008.02.090

Garcia, J. M., Scherer, T., Chen, J. A., Guillory, B., Nassif, A., Papusha, V., et al. (2013). Inhibition of cisplatin-induced lipid catabolism and weight loss by ghrelin in male mice. *Endocrinology.* 154 (9), 3118–3129. doi:10.1210/en.2013-1179

Ghafourifar, P., Klein, S., Schucht, O., Schenk, U., Pruschy, M., Rocha, S., et al. (1999). Ceramide induces cytochrome c release from isolated mitochondria: importance of mitochondrial redox state. *J. Biol. Chem.* 274, 6080–6084. doi:10.1074/jbc.274.10.6080

Gibellini, F., and Smith, T. K. (2010). The Kennedy pathway-De novo synthesis of phosphatidylethanolamine and phosphatidylcholine. *IUBMB Life.* 62 (6), 414–428. doi:10.1002/iub.337

Giordano, S., Morosi, L., Veglianese, P., Licandro, S., Frapolli, R., Zucchetti, M., et al. (2016). 3D mass spectrometry imaging reveals a very heterogeneous drug distribution in tumors. *Sci. Rep.* 6 (1), 37027–37028. doi:10.1038/srep37027

He, J., Luo, Z., Huang, L., He, J., Chen, Y., Rong, X., et al. (2015). Ambient mass spectrometry imaging metabolomics method provides novel insights into the action mechanism of drug candidates. *Anal. Chem.* 87 (10), 5372–5379. doi:10.1021/acs.analchem.5b00680

Hermansson, M., Hokynar, K., and Somerharju, P. (2011). Mechanisms of glycerophospholipid homeostasis in mammalian cells. *Prog. Lipid Res.* 50 (3), 240–257. doi:10.1016/j.plipres.2011.02.004

Hirsch, H. A., Iliopoulos, D., Joshi, A., Zhang, Y., Jaeger, S. A., Bulyk, M., et al. (2010). A transcriptional signature and common gene networks link cancer with lipid metabolism and diverse human diseases. *Canc. Cell.* 17 (4), 348–361. doi:10.1016/j.ccr.2010.01.022

Hishikawa, D., Hashidate, T., Shimizu, T., and Shindou, H. (2014). Diversity and function of membrane glycerophospholipids generated by the remodeling pathway in mammalian cells. *J. Lipid Res.* 55 (5), 799–807. doi:10.1194/jlr.R046094

Huang, C., and Freter, C. (2015). Lipid metabolism, apoptosis and cancer therapy. *Int. J. Mol. Sci.* 16 (1), 924–949. doi:10.3390/ijms16010924

Huang, J., Chen, F., Zhong, Z., Tan, H. Y., Wang, N., Liu, Y., et al. (2020). Interpreting the pharmacological mechanisms of huachansu capsules on hepatocellular carcinoma through combining network Pharmacology and experimental evaluation. *Front. Pharmacol.* 11, 414. doi:10.3389/fphar.2020.00414

Lehár, J., Krueger, A. S., Avery, W., Heilbut, A. M., Johansen, L. M., Price, E. R., et al. (2009). Synergistic drug combinations tend to improve therapeutically relevant selectivity. *Nat. Biotechnol.* 27 (7), 659–666. doi:10.1038/nbt.1549

Li, X., Chen, Y.-T., Hu, P., and Huang, W.-C. (2014). Fatostatin displays high antitumor activity in prostate cancer by blocking SREBP-regulated metabolic pathways and androgen receptor signaling. *Mol. Canc. Therapeut.* 13 (4), 855–866. doi:10.1158/1535-7163.MCT-13-0797

Li, W., Ren, L., Zheng, X., Liu, J., Wang, J., Ji, T., et al. (2020). 3-O-Acetyl-11-keto-β-boswellic acid ameliorated aberrant metabolic landscape and inhibited autophagy in glioblastoma. *Acta Pharm. Sin. B.* 10 (2), 301–312. doi:10.1016/j.apsb.2019.12.012

Lukowski, J. K., Weaver, E. M., and Hummon, A. B. (2017). Analyzing liposomal drug delivery systems in three-dimensional cell culture models using MALDI imaging mass spectrometry. *Anal. Chem.* 89 (16), 8453–8458. doi:10.1021/acs.analchem.7b02006

Luo, Z., He, J., Chen, Y., He, J., Gong, T., Tang, F., et al. (2013). Air flow-assisted ionization imaging mass spectrometry method for easy whole-body molecular imaging under ambient conditions. *Anal. Chem.* 85 (5), 2977–2982. doi:10.1021/ac400009s

Mao, C., and Obeid, L. M. (2008). Ceramidases: regulators of cellular responses mediated by ceramide, sphingosine, and sphingosine-1-phosphate. *BBA-Mol. Cell Biol. L.* 1781 (9), 424–434. doi:10.1016/j.bbalip.2008.06.002

Meng, Z., Yang, P., Shen, Y., Bei, W., Zhang, Y., Ge, Y., et al. (2009). Pilot study of huachansu in patients with hepatocellular carcinoma, nonsmall-cell lung cancer, or pancreatic cancer. *Cancer.* 115 (22), 5309–5318. doi:10.1002/cncr.24602

Muller, L., Kailas, A., Jackson, S. N., Roux, A., Barbacci, D. C., Schultz, J. A., et al. (2015). Lipid imaging within the normal rat kidney using silver nanoparticles by matrix-assisted laser desorption/ionization mass spectrometry. *Kidney Int.* 88 (1), 186–192. doi:10.1038/ki.2015.3

Ortega, J. A., Douglass, E. C., Feusner, J. H., Reynolds, M., Quinn, J. J., Finegold, M. J., et al. (2000). Randomized comparison of cisplatin/vincristine/fluorouracil and cisplatin/continuous infusion doxorubicin for treatment of pediatric hepatoblastoma: a report from the Children's Cancer Group and the Pediatric Oncology Group. *J. Clin. Oncol.* 18 (14), 2665–2675. doi:10.1200/JCO.2000.18.14.2665

Ow, Y. L. P., Green, D. R., Hao, Z., and Mak, T. W. (2008). Cytochrome c: functions beyond respiration. *Nat. Rev. Mol. Cell Biol.* 9 (7), 532–542. doi:10.1038/nrm2434

Perrotti, F., Rosa, C., Cicalini, I., Sacchetta, P., Del Boccio, P., Genovesi, D., et al. (2016). Advances in lipidomics for cancer biomarkers discovery. *Int. J. Mol. Sci.* 17 (12), 1992. doi:10.3390/ijms17121992

Qi, F., Inagaki, Y., Gao, B., Cui, X., Xu, H., Kokudo, N., et al. (2011). Bufalin and cinobufagin induce apoptosis of human hepatocellular carcinoma cells via Fas-and mitochondria-mediated pathways. *Canc. Sci.* 102 (5), 951–958. doi:10.1111/j.1349-7006.2011.01900.x

Reynolds, C. P., Maurer, B. J., and Kolesnick, R. N. (2004). Ceramide synthesis and metabolism as a target for cancer therapy. *Canc. Lett.* 206 (2), 169–180. doi:10.1016/j.canlet.2003.08.034

Roth, B. J., Krilov, L., Adams, S., Aghajanian, C. A., Bach, P., Braiteh, F., et al. (2013). Clinical cancer advances 2012: annual report on progress against cancer from the american society of clinical oncology. *J. Clin. Oncol.* 31 (1), 131–161. doi:10.1200/JCO.2012.47.1938

Sakakima, Y., Hayakawa, A., and Nakao, A. (2009). Phosphatidylcholine induces growth inhibition of hepatic cancer by apoptosis via death ligands. *Hepato. Gastroenterol.* 56 (90), 481–484.

Schütte, K., Schulz, C., and Malfertheiner, P. (2014). Hepatocellular carcinoma: current concepts in diagnosis, staging and treatment. *Gastrointest. tumors.* 1 (2), 84–92. doi:10.1159/000362583

Senchenkov, A., Litvak, D. A., and Cabot, M. C. (2001). Targeting ceramide metabolism-a strategy for overcoming drug resistance. *J. Natl. Cancer Inst.* 93 (5), 347–357. doi:10.1093/jnci/93.5.347

Shen, S., Zhang, Y., Wang, Z., Zhang, R., and Gong, X. (2014). Bufalin induces the interplay between apoptosis and autophagy in glioma cells through endoplasmic reticulum stress. *Int. J. Biol. Sci.* 10 (2), 212. doi:10.7150/ijbs.8056

Storck, E. M., Özbalci, C., and Eggert, U. S. (2018). Lipid cell biology: a focus on lipids in cell division. *Annu. Rev. Biochem.* 87, 839–869. doi:10.1146/annurev-biochem-062917-012448

Struzik, Z. J., Weerts, A. N., Storch, J., and Thompson, D. H. (2020). Stereospecific synthesis of phosphatidylglycerol using a cyanoethyl phosphoramidite precursor. *Chem. Phys. Lipids.* 231, 104933. doi:10.1016/j.chemphyslip.2020.104933

Strydom, N., Gupta, S. V., Fox, W. S., Via, L. E., Bang, H., Lee, M., et al. (2019). Tuberculosis drugs' distribution and emergence of resistance in patient's lung lesions: a mechanistic model and tool for regimen and dose optimization. *PLoS Med.* 16 (4), e1002773. doi:10.1371/journal.pmed.1002773

Su, X., Dong, C., Zhang, J., Su, L., Wang, X., Cui, H., et al. (2014). Combination therapy of anti-cancer bioactive peptide with Cisplatin decreases chemotherapy dosing and toxicity to improve the quality of life in xenograft nude mice bearing human gastric cancer. *Cell Biosci.* 4 (1), 7.doi:10.1186/2045-3701-4-7

Sun, C., Li, T., Song, X., Huang, L., Zang, Q., Xu, J., et al. (2019). Spatially resolved metabolomics to discover tumor-associated metabolic alterations. *P. Natl. Acad. Sci. USA.* 116 (1), 52–57. doi:10.1073/pnas.1808950116

Thomas, M. B., and Zhu, A. X. (2005). Hepatocellular carcinoma: the need for progress. *J. Clin. Oncol.* 23 (13), 2892–2899. doi:10.1200/JCO.2005.03.196

Ullman, M. D., and Radin, N. S. (1974). The enzymatic formation of sphingomyelin from ceramide and lecithin in mouse liver. *J. Biol. Chem.* 249 (5), 1506–1512.

Vance, D. E. (2013). Physiological roles of phosphatidylethanolamine N-methyltransferase. *BBA-Mo.l Cell Biol. L.* 1831, 626–632. doi:10.1016/j.bbalip.2012.07.017

Vance, D. E., Walkey, C. J., and Cui, Z. (1997). Phosphatidylethanolamine N-methyltransferase from liver. *BBA-Mo.l Cell Biol. L.* 1348, 142–150. doi:10.1016/j.bbalip.2012.07.017

Vance, J. E., and Steenbergen, R. (2005). Metabolism and functions of phosphatidylserine. *Prog. Lipid Res.* 44 (4), 207–234. doi:10.1016/j.plipres.2005.05.001

Vander Heiden, M. G., and DeBerardinis, R. J. (2017). Understanding the intersections between metabolism and cancer biology. *Cell.* 168 (4), 657–669. doi:10.1016/j.cell.2016.12.039

Wang, J., Qiu, S., Chen, S., Xiong, C., Liu, H., Wang, J., et al. (2015). MALDI-TOF MS imaging of metabolites with a N-(1-naphthyl) ethylenediamine dihydrochloride matrix and its application to colorectal cancer liver metastasis. *Anal. Chem.* 87 (1), 422–430. doi:10.1021/ac504294s

Won, J. S., and Singh, I. (2006). Sphingolipid signaling and redox regulation. *Free Radical Bio. Med.* 40 (11), 1875–1888. doi:10.1016/j.freeradbiomed.2006.01.035

Woodfield, S. E., Shi, Y., Patel, R. H., Jin, J., Major, A., Sarabia, S. F., et al. (2017). A novel cell line based orthotopic xenograft mouse model that recapitulates human hepatoblastoma. *Sci. Rep.* 7 (1), 17751. doi:10.1038/s41598-017-17665-8

Yang, K., and Han, X. (2016). Lipidomics: techniques, applications, and outcomes related to biomedical sciences. *Trends Biochem. Sci.* 41 (11), 954–969. doi:10.1016/j.tibs.2016.08.010

Yang, X., Zhang, Y., Zhang, L., Zhang, L., and Mao, J. (2008). Silencing alpha-fetoprotein expression induces growth arrest and apoptosis in human hepatocellular cancer cell. *Canc. Lett.* 271 (2), 281–293. doi:10.1016/j.canlet.2008.06.017

Zemski Berry, K. A., Hankin, J. A., Barkley, R. M., Spraggins, J. M., Caprioli, R. M., and Murphy, R. C. (2011). MALDI imaging of lipid biochemistry in tissues by mass spectrometry. *Chem. Rev.* 111 (10), 6491–6512. doi:10.1021/cr200280p

Zhang, J., Fujimoto, J., Zhang, J., Wedge, D. C., Song, X., Zhang, J., et al. (2014). Intratumor heterogeneity in localized lung adenocarcinomas delineated by multiregion sequencing. *Science.* 346 (6206), 256–259. doi:10.1126/science.1256930

Zhang, S., Zhuang, J., Yue, G., Wang, Y., Liu, M., Zhang, B., et al. (2017). Lipidomics to investigate the pharmacologic mechanisms of ginkgo folium in the hyperuricemic rat model. *J. Chromatogr. B.* 1060, 407–415. doi:10.1016/j.jchromb.2017.06.037

Zhang, J., Hong, Y., Jiang, L., Yi, X., Chen, Y., Liu, L., et al. (2020). Global metabolomic and lipidomic analysis reveal the synergistic effect of bufalin in combination with cinobufagin against HepG2 cells. *J. Proteome Res.* 19 (2), 873–883. doi:10.1021/acs.jproteome.9b00681

Conflict of Interest: The authors declare that the research was conducted in the absence of any commercial or financial relationships that could be construed as a potential conflict of interest.